

# The Size and Shape of Local Voids

Manolis Plionis<sup>1</sup> & Spyros Basilakos<sup>2</sup>

<sup>1</sup> *Institute of Astronomy & Astrophysics, National Observatory of Athens, I.Metaxa & B.Pavlou, Palaia Penteli, 152 36, Athens, Greece*

<sup>2</sup> *Astrophysics Group, Imperial College London, Blackett Laboratory, Prince Consort Road, London SW7 2BW, UK*

27 October 2018

## ABSTRACT

We study the size and shape of low density regions in the local universe which we identify in the smoothed density field of the PSCz flux limited IRAS galaxy catalogue. After quantifying the systematic biases that enter in the detection of voids using our data set and method, we identify, using a smoothing length of  $5 h^{-1}$  Mpc, 14 voids within  $80 h^{-1}$  Mpc (having volumes  $\geq 10^3 h^{-3}$  Mpc<sup>3</sup>) and using a smoothing length of  $10 h^{-1}$  Mpc, 8 voids within  $130 h^{-1}$  Mpc (having volumes  $\geq 8 \times 10^3 h^{-3}$  Mpc<sup>3</sup>). We study the void size distribution and morphologies and find that there is roughly an equal number of prolate and oblate-like spheroidal voids. We compare the measured PSCz void shape and size distributions with those expected in six different CDM models and find that only the size distribution can discriminate between models. The models preferred by the PSCz data are those with intermediate values of  $\sigma_8$  ( $\simeq 0.83$ ), independent of cosmology.

**Keywords:** cosmology:theory - galaxies: general - large-scale structure of universe - Infrared: galaxies

## 1 INTRODUCTION

Many authors have claimed that low density regions (voids) are the most common features of the large scale structure of the universe owing to the fact that they occupy more than a half of its volume. Individual voids and their properties have been investigated by different authors (cf. Jo veer et al. 1978; Kirshner et al. 1981; Rood 1981 and references that he gives). Since their creation has been attributed to the effects of gravitational instability (cf. Zeldovich, Einasto & Shandarin 1982; Coles, Melott & Shandarin 1993; Peebles 2001 and references therein), the distribution of voids on large scales could provide important constraints on models of structure formation. From N-body simulations it has become evident that in the hierarchical structure formation scenario, matter collapses and forms high density objects, like clusters and superclusters, and enhance the underdense regions between them (cf. Melott et al. 1983). Therefore, if the above view is correct then the morphological and statistical properties of voids (size, shape) should depend on the initial power spectrum  $P(k)$  and on the density parameter  $\Omega_0$  (cf. White 1979; Melott 1987; Einasto, Einasto & Gramann 1989; Reg s & Geller 1991; Ryden & Melott 1996). Blaes, Goldreich & Villumsen (1990) and Van de Weygaert & Van Kampen (1993) studied the morphological properties of voids and found, that the latter structures become nearly spherical in their very underdense internal regions.

In order to study in an objective manner the distribution of voids and their physical properties it is necessary to develop objective void-finding algorithms and to apply them onto well controlled data. Such attempts were pioneered by Kauffmann & Fairall (1991), Kauffmann & Melott (1992) and more recently by El-Ad, Piran & da Costa (1996), El-Ad & Piran (1997) and Stavrev (2000). El-Ad, Piran & da Costa (1997) applied their void-finding algorithm to the IRAS 1.2Jy galaxy catalogue and found, within  $80 h^{-1}$  Mpc, 15 voids with an average diameter of  $40 \pm 6 h^{-1}$  Mpc. M ller et al. (2001) have also studied the distribution of voids and their sizes using the large Las Campanas Redshift Survey and compared their properties with CDM simulations. They found that although the void-size distribution provides important information on the large-scale distribution of matter, galaxy biasing seems more important in defining voids than differences between the cosmological models.

In this paper we use the PSCz-IRAS redshift survey in order to measure the void size and shape distributions in the local universe and to investigate whether these distributions can be used as cosmological probes. The plan of the paper is the following: In section 2 we briefly describe the PSCz data. In section 3 we present the void identification and shape determination procedure, the systematic effects that affect the PSCz void detection and our results. We compare our PSCz results with the corresponding ones of six cosmological models in section 4 and finally in section 5 we draw our conclusions.

## 2 THE PSCZ GALAXY SAMPLE

In our analysis we use the recently completed IRAS flux-limited 60- $\mu\text{m}$  redshift survey (PSCz) which is described in Saunders et al. (2000). The PSCz catalogue contains  $\sim 15500$  galaxies with flux  $S_{\text{lim}} \geq 0.6$  Jy covering the  $\sim 84\%$  of the sky.

To construct an unbiased continuous density field we have to take into account the well-known degradation of sampling as a function of distance due to the fact that the PSCz catalogue is a flux limited sample. This is done by weighting each galaxy by the inverse selection function, assuming that the fainter unobserved galaxies are spatially correlated with the bright observed ones. Note that the selection function is defined as the fraction of the galaxy number density that is observed above the flux limit at some distance  $r$ . We estimate the selection function by using the functional form of the IRAS galaxy luminosity function of Saunders et al. (1990) with parameters:  $L_* = 10^{8.45} h^2 L_\odot$ ,  $\sigma = 0.711$ ,  $\alpha = 1.09$  and  $C = 0.0308$  (Rowan-Robinson et al. 2000).

In order to treat the 16% excluded sky (galactic plane, high cirrus emission areas and unobserved regions) we use the PSCz data reduction of Branchini et al. (1999), in which they followed the Yahil et al. (1991) method to fill the galactic plane region. This method consists of dividing the Galactic strip into 36 bins of  $10^\circ$  in longitude and in distance bins of 1000 km/sec width. The galaxy distribution in each bin is then simulated by random sampling the adjacent galactic latitude and distance strips. Therefore the local density fluctuations are extrapolated in the galactic plane. In the high Galactic latitudes, the unobserved regions are filled homogeneously with simulated galaxies following the PSCz radial selection function.

Finally, in this kind of analysis it is essential to transform redshifts to 3D distances in order to minimise the so called ‘‘Kaiser’’ effect. This effect can be understood by noting that the distribution of galaxies in redshift space is a distorted representation of that in real comoving space due to their peculiar velocities (Kaiser 1987). In this paper we use the 3D distances determined by the iterative algorithm of Branchini et al. (1999) in which they assume that (a) peculiar velocities are produced by gravitational instability (b) non-linear effects can be neglected once the density field is smoothed and (c) galaxies and mass fluctuations are related through a linear biasing relation with  $\beta = 0.5^*$ . This value of  $\beta$  is strongly suggested from the Branchini et al. (2001) comparison between the PSCz density field and the SFI galaxy velocities (cf. Haynes et al. 1999).

## 3 PSCZ VOIDS

### 3.1 Smoothing Procedure

For the purpose of this study we need to derive from the discrete distribution of PSCz galaxies a smooth contin-

uous density field. This is realized by utilizing a Gaussian kernel on a  $N^3$  grid and using two smoothing radii, namely  $R_{\text{sm}} = 5 h^{-1}$  Mpc and  $10 h^{-1}$  Mpc, to probe essentially different void sizes.

As we verified in Basilakos, Plionis & Rowan-Robinson (2001), the coupling between the selection function and the constant radius smoothing, results in a distorted smoothed density distribution, especially at large distances. Gaussian spheres, centered on distant cells, overestimate the true density in regions where galaxies are detected (due to the heavy selection function weighting), while in underdense regions they underestimate the true density. Using numerical simulations, Basilakos et al. (2001) identified the depth out to which these distortions are relatively small and developed a phenomenological approach to correct such biases. Their procedure is effective in recovering especially the high-density end of the probability density function (*pdf*).

In the present study we use such a corrected density field and based on the above analysis we extend our smoothing procedure out to  $r_{\text{max}}$ , where  $r_{\text{max}} = 130$  and  $170 h^{-1}$  Mpc respectively for the two smoothing radii while the size of each cell is set equal to  $R_{\text{sm}}$ . We will investigate further possible systematic effects of our method and data by using a Monte-Carlo approach in section 3.4.

### 3.2 Void Detection

In order to find our void candidates we select all grid-cells with  $|b| \geq 10^\circ$  and with an overdensity under a chosen threshold and then join together those having common boundaries. Due to the fact that voids should be identified as low density regions, the threshold value of the overdensity ( $\delta_{\text{th}}$ ) could be defined directly from the probability density function as its 10%-ile value ( $\delta_{\text{th}} = -0.68$  and  $-0.39$  for the  $R_{\text{sm}} = 5h^{-1}\text{Mpc}$  and  $R_{\text{sm}} = 10h^{-1}\text{Mpc}$  respectively). Using higher values of  $\delta_{\text{th}}$  we tend to connect voids and percolate underdense regions through the whole volume. Finally, we choose to analyse the above candidate voids for two different limiting distances, namely  $r_{\text{lim}} \simeq 80h^{-1}\text{Mpc}$  for  $R_{\text{sm}} = 5 h^{-1}$  Mpc, and  $r_{\text{lim}} \simeq 130 h^{-1}$  Mpc for  $R_{\text{sm}} = 10 h^{-1}$  Mpc respectively in order to avoid distance dependent systematic effects (see section 3.4 and figure 1).

### 3.3 Shape Statistics

Shapes are estimated for those ‘‘voids’’ that consist of 8 or more connected underdense cells, utilizing the moments of inertia ( $I_{ij}$ ) method to fit the best triaxial ellipsoid to the data (cf. Carter & Metcalfe 1980; Plionis, Barrow & Frenk 1991; Basilakos et al. 2001). We diagonalize the inertia tensor

$$\det(I_{ij} - \lambda^2 M_3) = 0 \quad (M_3 \text{ is } 3 \times 3 \text{ unit matrix}), \quad (1)$$

obtaining the eigenvalues  $\alpha_1, \alpha_2, \alpha_3$  (where  $\alpha_1$  is the semi-major axes) from which we define the shape of the configuration since, the eigenvalues are directly related to the three principal axes of the fitted ellipsoid. The

\*  $\beta = \Omega_0^{0.6}/b_{\text{IRAS}}$ , with  $b_{\text{IRAS}}$  the IRAS bias factor. Our results remain qualitatively the same also for  $\beta = 1$ .

volume of each void is then  $V = \frac{4\pi}{3}\alpha_1\alpha_2\alpha_3$ . According to the logic of our void-finder, 8 underdense cells in a row can be connected to form a ‘void’, which would then appear as purely prolate.

The shape statistic procedure, that we use, is based on a differential geometry approach, introduced by Sahni et al (1998) [for application to astronomical data see Basilakos et al. 2001]. Here we review only some basic concepts. A set of three shapefinders are defined having dimensions of length;  $\mathcal{H}_1 = VS^{-1}$ ,  $\mathcal{H}_2 = SC^{-1}$  and  $\mathcal{H}_3 = C$ , with  $S$  the surface area and  $C$  the integrated mean curvature. Then it is possible to define a set of two dimensional shapefinders  $K_1$  and  $K_2$ , as:

$$K_1 = \frac{\mathcal{H}_2 - \mathcal{H}_1}{\mathcal{H}_2 + \mathcal{H}_1} \quad (2)$$

and

$$K_2 = \frac{\mathcal{H}_3 - \mathcal{H}_2}{\mathcal{H}_3 + \mathcal{H}_2}, \quad (3)$$

normalized to give  $\mathcal{H}_i = R$  ( $K_{1,2} = 0$ ) for a sphere of radius  $R$ . Therefore, based on these shapefinders we can characterise the morphology of cosmic structures (underdense or overdense regions) according to the following categories: (i) oblate-like ellipsoids for  $K_1/K_2 > 1$ ; (ii) prolate-like ellipsoids for  $K_1/K_2 < 1$ ; (iii) triaxial for  $K_1/K_2 \simeq 1$  and (iv) spheres for  $\alpha_1 \simeq \alpha_2 \simeq \alpha_3$  and thus  $(K_1, K_2) \simeq (0, 0)$ . For the quasi-spherical objects the ratio  $K_1/K_2$  measures the deviation from pure sphericity.

### 3.4 Test for systematic errors

We run a large number of Monte-Carlo simulations in which we destroy the intrinsic PSCz galaxy clustering by randomising the angular coordinates of the galaxies while keeping their distances and therefore their selection function unchanged. On this intrinsically random galaxy distribution, utilizing the procedure described before, we identify the expected random voids,  $N_{\text{rand}}$ , which are due to our void-identification method itself. In figure 1 we plot for the different smoothing radii, the probability of detecting real voids in the PSCz data, defined as  $\mathcal{P} = 1 - N_{\text{rand}}/N_{\text{PSCz}}$ , as well as the number of real PSCz voids,  $N_{\text{PSCz}}$ . In the presence of negligible systematic biases in our method and data, the above selection process should result in  $\mathcal{P} \simeq 1$ , at all distances.

We find that the number of random voids increases with distance, a fact which should be attributed to the coupling of the PSCz selection function (ie., the degradation of the observed mean galaxy density as a function of distance which produces an inherently noisier density field at large distances) and the constant radius smoothing. Our phenomenological method of recovering the true density field (Basilakos et al. 2001) is multiplicative in nature and thus it is unable to correct the low and zero density cells. Therefore, the lower part of the *pdf* cannot be recovered efficiently. In particular we find that for  $R_{\text{sm}} = 5h^{-1}\text{Mpc}$  smoothing radius (figure 1, squares), we have  $\mathcal{P} > 0.8$  for detecting real voids within  $r \leq 80^{-1}\text{Mpc}$  while for the  $R_{\text{sm}} = 10h^{-1}\text{Mpc}$  smoothing radius (figure 1, circles), a similar probability is found

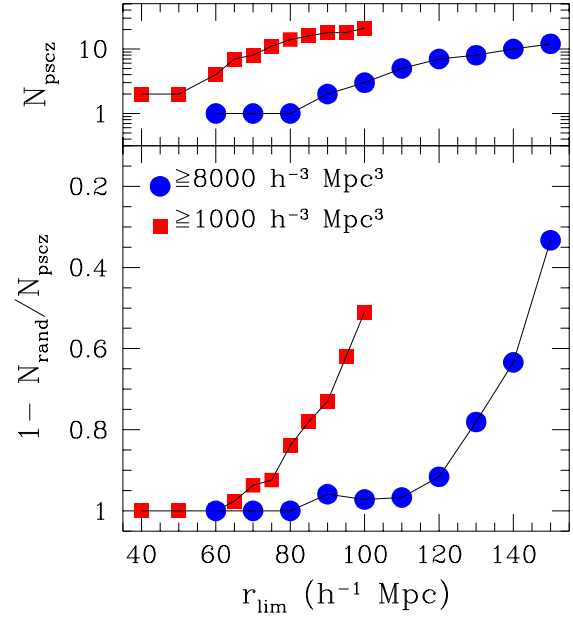


**Figure 1.** Statistical significance of our void detection procedure as a function of distance using either  $R_{\text{sm}} = 5h^{-1}\text{Mpc}$  or  $R_{\text{sm}} = 10h^{-1}\text{Mpc}$ .

within  $r \leq 130^{-1}\text{Mpc}$ . Note that for the largest voids in our sample this probability is much larger ( $>0.98$ ).

### 3.5 The PSCz Void Cosmography

In figure 2 we plot the smoothed PSCz galaxy distribution on the supergalactic plane out to  $90 h^{-1}\text{Mpc}$ . The contour step is  $\Delta\delta = 0.6$ , starting from  $\delta_{\text{th}} = -0.68$  while the  $\delta = 0$  level appears as a thick continuous line. All major known clusters are present, like the Virgo cluster at  $X_{\text{sup}} \simeq -5$ ,  $Y_{\text{sup}} \simeq 5$ ; the Hydra-Centaurus at  $X_{\text{sup}} \simeq 35$ ,  $Y_{\text{sup}} \simeq 15$ ; the Perseus at  $X_{\text{sup}} \simeq 50$ ,  $Y_{\text{sup}} \simeq -20$  and the Coma at  $X_{\text{sup}} \simeq 0$ ,  $Y_{\text{sup}} \simeq 70$ . We also plot the voids that we have detected as big circles while as crosses we mark the IRAS 1.2Jy voids found by El-Ad et al. (1997). We observe that our respective voids have almost identical positions. However, we do not detect two IRAS 1.2Jy voids, which in one case is due to a slight difference in the void  $Z_{\text{sup}}$ -position (our void No5 in table 1) and in the other it is probably due to our adopted overdensity threshold. Furthermore, the underdense region at the upper right section of the density map extends to higher  $Z_{\text{sup}}$  and constitutes a large void (our No 12).

Details for those voids that consist of 8 or more cells are presented in table 1 and 2 for both smoothing radii; the different columns being self explanatory. Evidently 8 voids out of 14 are prolate-like ellipsoids and the rest oblate-like. While from table 2, we see that we have a slight excess of oblate-like voids, with one purely triaxial void ( $K_1/K_2 \simeq 1$ ). Regarding extreme shaped voids, we have found, in the  $R_{\text{sm}} = 5 h^{-1}\text{Mpc}$  field, two very prolate voids (see table 1: void 2 and 9), while in the

**Table 1.** Detected voids in the  $R_{sm} = 5 h^{-1}$  Mpc density field for  $\delta \leq -0.69$  (corresponding to the 10%-ile) with  $V \geq 10^3 h^{-3}$  Mpc<sup>3</sup> ( $N_{\text{cell}} \geq 8$ ) and  $r \leq 80 h^{-1}$  Mpc. The different columns are self-explanatory with column 3 being the distance of the void center and column 10 the void semi-major axis. The Local Void is No13 and the Sculptor Void is No4.

N	Volume ( $10^3 h^{-3}$ Mpc <sup>3</sup> )	d ( $h^{-1}$ Mpc)	$X_{sup}$	$Y_{sup}$	$Z_{sup}$	$K_1$	$K_2$	$K_1/K_2$	$\alpha_1$ ( $h^{-1}$ Mpc)
1	8.6	77.4	14.8	-73.2	-20.6	0.040	0.060	0.67	20.7
2	2.4	72.6	-6.9	-58.4	42.5	0.073	0.205	0.35	19.9
3	12.6	78.5	69.6	-28.9	22.0	0.033	0.045	0.72	22.1
4	62.0	78.2	-67.4	-39.5	-4.8	0.039	0.042	0.94	36.8
5	3.8	33.9	-13.8	-24.9	-18.4	0.017	0.014	1.21	12.0
6	1.8	73.9	27.6	-28.2	62.5	0.070	0.041	1.70	10.9
7	2.2	38.6	-17.2	-16.7	30.3	0.021	0.031	0.67	11.6
8	8.9	70.0	13.6	34.1	-59.6	0.028	0.024	1.17	17.3
9	1.4	63.4	-42.9	33.3	-32.7	0.078	0.286	0.27	19.5
10	1.2	50.4	18.5	46.5	-6.0	0.102	0.063	1.61	11.1
11	1.8	60.6	39.0	45.1	-11.1	0.033	0.032	1.03	10.6
12	16.4	64.5	37.8	49.4	17.1	0.084	0.101	0.83	29.8
13	25.4	51.2	-10.6	30.3	39.9	0.079	0.042	1.86	26.6
14	1.9	71.6	-8.8	63.2	32.5	0.029	0.034	0.85	11.1

**Table 2.** Detected voids in the  $R_{sm} = 10 h^{-1}$  Mpc density field for  $\delta \leq -0.39$  (corresponding to the 10%-ile) with  $V \geq 8 \times 10^3 h^{-3}$  Mpc<sup>3</sup> ( $N_{\text{cell}} \geq 8$ ) and  $r \leq 130 h^{-1}$  Mpc.

N	Volume ( $10^4 h^{-3}$ Mpc <sup>3</sup> )	d ( $h^{-1}$ Mpc)	$X_{sup}$	$Y_{sup}$	$Z_{sup}$	$K_1$	$K_2$	$K_1/K_2$	$\alpha_1$ ( $h^{-1}$ Mpc)
1	2.5	129.6	-48.8	-115.3	33.5	0.063	0.050	1.27	28.1
2	63.8	117.3	37.8	-107.4	-27.9	0.077	0.048	1.60	81.7
3	1.2	58.5	-28.5	-50.9	5.0	0.067	0.059	1.14	23.0
4	0.9	103.6	72.8	-38.4	62.9	0.063	0.153	0.41	27.6
5	1.6	109.4	86.8	-23.3	-62.2	0.016	0.016	1.00	19.9
6	7.7	97.8	-80.3	-43.2	35.4	0.063	0.193	0.33	61.7
7	2.8	111.3	-6.4	72.9	-83.9	0.048	0.044	1.09	28.5
8	34.0	86.8	53.1	46.7	50.2	0.055	0.155	0.36	92.6

$R_{sm} = 10 h^{-1}$  Mpc field, we again find two such prolate-like voids (see table 2: voids 6 and 8).

The median value of the semi-major void axes is  $\sim 20 h^{-1}$  Mpc and  $\sim 28 h^{-1}$  Mpc for  $R_{sm} = 5 h^{-1}$  Mpc and  $R_{sm} = 10 h^{-1}$  Mpc fields respectively, in good agreement with the results of El-Ad et al (1997).

If we had used the redshift space PSCz density field we would have found the same voids, with a similar size distribution but biased towards prolate shapes.

#### 4 COMPARISON WITH COSMOLOGICAL MODELS

We use mock PSCz catalogues (Branchini et al. 1999) generated from six large cosmological N-body simulations of Cole et al. (1998), in order to investigate whether void properties (shapes and numbers) can discriminate between models. We consider six different cold dark matter models, which are presented in table 3.

For each cosmological model we average results over 10 nearly independent mock PSCz catalogues extending out to a radius of  $170 h^{-1}$ Mpc which were produced by Enzo Branchini (see Branchini et al 1999). Good care was taken to center the catalogues to suitable LG-like observers (having similar to the observed Local Group velocity, shear and overdensity). Note that due to our ignorance in assigning galaxy formation sites to the DM

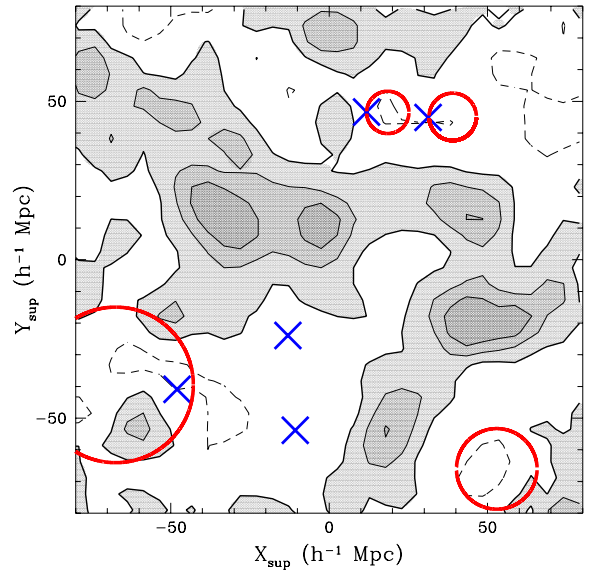


**Figure 2.** The smooth PSCz density field on the Supergalactic Plane out to  $90 h^{-1}$ Mpc. Large circles represent our detected voids (with sizes proportional to their volume) and crosses represent those of El-Ad et al. (1997) (with  $-17 < Z_{sup} < 17 h^{-1}$ ).

**Table 3.** Model parameters. The first four are normalized by the observed cluster abundance at zero redshift, ie.,  $\sigma_8 = 0.55\Omega_{\nu}^{-0.6}$  (Eke, Cole, & Frenk 1996), while the fifth is COBE normalized with  $\sigma_8 = 1.35$ .

Model	$\Omega_m$	$\Omega_{\Lambda}$	$\Gamma$	$\sigma_8$
$\Lambda_{\text{CDM1}}$	0.3	0.7	0.25	1.13
$\Lambda_{\text{CDM2}}$	0.5	0.5	0.25	0.83
$\tau_{\text{CDM}}$	1.0	0.0	0.25	0.55
$\text{O}_{\text{CDM}}$	0.5	0.0	0.25	0.83
$\text{C}_{\text{CDM}}$	1.0	0.0	0.5	1.35
$\text{S}_{\text{CDM}}$	1.0	0.0	0.5	0.55

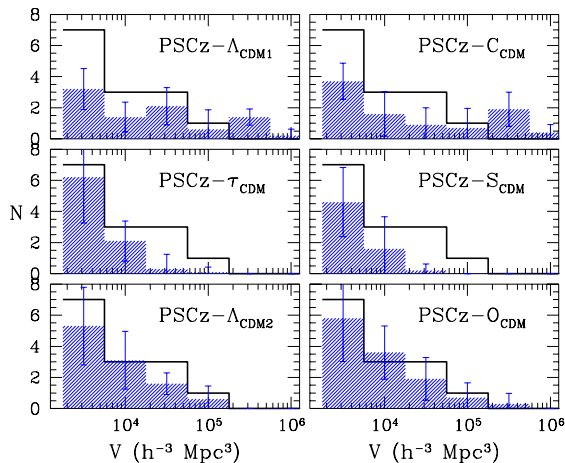


**Figure 3.** Void-size distribution comparison between the PSCz and look-alikes generated from 6 cosmological models. The model results are represented by the hatched regions and the errorbars represent the scatter among the 10 realizations of each model.

halo distribution and for a consistent treatment of all models, a biasing factor of 1 has been used in generating the PSCz look-alikes.

We analyse the mock PSCz catalogues density fields (with  $R_{sm} = 5 h^{-1}$  Mpc) in the same fashion as that of the observed PSCz catalogue. We find that the void shape distribution cannot discriminate among the different models, a result which is similar with the shape-spectrum analysis of superclusters (see Basilakos et al 2001).

In figure 3 we plot the PSCz void-size frequency distribution in logarithmic bins and compare it with the outcome of all six models (hatched regions). We see that the models with similar value of  $\sigma_8$  produce similar void-size distributions. We have verified this by using a Kolmogorov-Smirnov test on the unbinned distribution of void-sizes from all 10 realizations. Indeed, all pairs of model void-size distributions are excluded from being drawn from the same parent population at a high significance level ( $> 99.9\%$ ), except for pairs that have similar values of  $\sigma_8$ , ie.,  $\Lambda_{\text{CDM1}}-\text{C}_{\text{CDM}}$ ,  $\Lambda_{\text{CDM2}}-\text{O}_{\text{CDM}}$  and  $\text{S}_{\text{CDM}}-\tau_{\text{CDM}}$ , which appear absolutely consistent among them.

Since in the model-data comparison we deal with

**Table 4.**  $\chi^2$  probability of significant differences between the model-model or model-data void-size distributions. Each probability value corresponds to the pair formed between the indicated model or data in the first column and the first row. In bold we indicate the results of the PSCz-model comparison.

	$\Lambda_{\text{CDM1}}$	$\text{C}_{\text{CDM}}$	$\tau_{\text{CDM}}$	$\text{S}_{\text{CDM}}$	$\Lambda_{\text{CDM2}}$	$\text{O}_{\text{CDM}}$
<b>PSCz</b>	<b>0.002</b>	<b>0.006</b>	<b>0.001</b>	<b>0.000</b>	<b>0.195</b>	<b>0.870</b>
$\Lambda_{\text{CDM1}}$		0.797	0.008	0.042	0.020	0.053
$\text{C}_{\text{CDM}}$			0.114	0.428	0.221	0.302
$\tau_{\text{CDM}}$				0.906	0.166	0.408
$\text{S}_{\text{CDM}}$					0.007	0.014
$\Lambda_{\text{CDM2}}$						0.986

only one realization of the Local Void distribution and since we have only 14 such voids, a rather small number for the K-S test to give reliable results (as we have verified using the K-S test with single model realizations), we quantify the differences between models and data by performing a standard binned  $\chi^2$  test, taking into account the scatter from the 10 different PSCz-like realizations. These probabilities are presented in table 4. Note the limitations of this test due to the large covariance between bins. However, by applying it to the model distributions, for which we have reliable KS probabilities, we can assess its reliability.

Comparing the void-size distributions of the models among themselves we see that the  $\chi^2$  test is less sensitive to differences among the models with respect to the K-S test. With the exception of the  $\text{C}_{\text{CDM}}$  and  $\tau_{\text{CDM}}$  models, which cannot be discriminated against, the other models follow the overall behaviour found by the K-S test when it was applied to the voids of all 10 realizations.

Regarding the comparison between the PSCz and model voids, we see from both figure 3 and table 4 that the only models that fit the PSCz data, at a high significance level, are models with  $\sigma_8 = 0.83$ ; ie., the  $\Lambda_{\text{CDM2}}$  and  $\text{O}_{\text{CDM}}$ , confirming the visual impression. Equivalent results are found by comparing the largest or most extremely shaped void of each realization with that of the PSCz data. This is not to say that an  $\Omega_{\nu} = 0.5$  should be preferred but rather that a  $\sigma_8 \simeq 0.83$  CDM model is consistent with the data (similar results are found from the whole *pdf* study; Plionis & Basilakos 2001).

## 5 CONCLUSIONS

We have studied the properties of voids detected in the smoothed PSCz galaxy density field as connected regions under some overdensity threshold. We have investigated the biases that enter in the detection of voids using our procedure and the PSCz smoothed density field. We reliably detect 14 voids within  $80 h^{-1}$  Mpc, in the  $R_{sm} = 5 h^{-1}$  Mpc smoothed field, having a median semi-major axis of  $\sim 20 h^{-1}$  Mpc and 8 voids in the relatively more distant Universe ( $r \leq 130 h^{-1}$  Mpc) for the  $R_{sm} = 10 h^{-1}$  Mpc smoothed field, having a median semi-major axis  $\sim 28 h^{-1}$  Mpc. Finally, we have

compared our PSCz void-size distribution with the corresponding ones generated from six cosmological models and we find that the CDM models that best reproduce the PSCz results are those with  $\sigma_8 \simeq 0.83$ , independent of cosmology.

## ACKNOWLEDGMENTS

S.Basilakos has benefited from discussions with P.Coles. M.Plionis acknowledges the hospitality of the Astrophysics Group of Imperial College. We both thank E.Branchini for providing us with his reconstructed PSCz galaxy distribution and the PSCz look-alikes. We both thank the referee, M.Vogeley, for helpful comments and suggestions.

## REFERENCES

- Basilakos, S., Plionis, M., Rowan-Robinson, M., 2001, MNRAS, 323, 47
- Blaes, O. M., Goldreich, P. M., Villumsen, J. V., 1990, ApJ, 361, 331
- Branchini, E., et al., 1999, MNRAS, 308, 1
- Branchini, E., Freudling, W., Da Costa, L.N., Frenk, C.S., Giovanelli, R., Haynes, M.P., Salzer, J.J., Wegner, G., Zehavi, I., 2001, MNRAS, 326, 1191
- Carter, D. & Metcalfe, J., 1980, MNRAS, 191, 325
- Cole, S., Hatton, S., Weinberg, D. H., Frenk, C. S., 1998, MNRAS, 300, 945
- Coles, P., Melott, A. L., Shandarin, S. F., 1993, MNRAS, 260, 765
- Einasto, J., Einasto, M., Gramann, M., 1989, MNRAS, 238, 155
- Eke, V., Cole, S., Frenk, C. S., 1996, MNRAS, 282, 263
- El-Ad, H., & Piran, T., 1997, ApJ, 491, 421
- El-Ad, H., Piran, T., da Costa, L. N., 1997, MNRAS, 287, 790
- El-Ad, H., Piran, T., da Costa, L. N., 1996, ApJ, 462, L13
- Haynes, M.P., Giovanelli, R., Salzer, J.J., Wegner, G., Freudling, W., da Costa, L.N., Herter, T., Vogt, N.P., 1999, AJ, 117, 1668
- Jõeveer, M., Einasto, J., Tago, E., 1978, MNRAS, 185, 35
- Kauffmann, G., Fairall, A.P., 1991, MNRAS, 248, 313
- Kauffmann, G., Melott, A.L., 1992, ApJ, 393, 415
- Kirshner, R.P., Oemler A., Schechter, P.L., Shectman, S.A., 1981, ApJ, 248, L57
- Kaiser, N., 1987, ApJ, 284, L9 A&A, 301, 329
- Melott, A. L., Einasto, J., Saar, E., Suisalu, I., Klypin, A. A., Shandarin, S. F., 1983, PhRvL, 51, 935
- Melott, A. L., 1987, MNRAS, 228, 1001
- Melott, A. L., & Shandarin, S. F., 1993, ApJ, 410, 469
- Müller, V., Arbabi-Bidgoli, S., Einasto, J., Tucker, D., 2000, MNRAS, 318, 280
- Peebles, P.J.E., 2001, ApJ, *in press*
- Plionis, M., Barrow J.D., Frenk, C.S., 1991, MNRAS, 249, 662
- Plionis, M., & Basilakos, S., 2001, MNRAS, 327, L32
- Regös, E., & Geller, M., 1991, ApJ, 377, 14
- Rood, H. J., 1981, RPPh, 44, 1077
- Rowan-Robinson, M., et al., 2000, MNRAS, 314, 37
- Ryden, B. S., & Melott, A. L., 1996, ApJ, 470, 160
- Sahni, V., Sathyapokash, B. S., Shandarin, S., 1998a, ApJ, 495, L5
- Saunders, W., Rowan-Robinson, M., Lawrence, A., Efstathiou, G., Kaizer, N., Ellis, R. S., Frenk, C. S., 1990, MNRAS, 242, 318
- Stavrev, K.Y., 2000, A&AS, 144, 323
- Saunders, W., et al., 2000, MNRAS, 317, 55
- Van de Weygaert, R. & Van Kampen, E., 1993, MNRAS, 263, 281
- White, S.D.M., 1979, MNRAS, 186, 145
- Yahil A., Strauss M., Davis M., Huchra J.P., 1991, ApJ, 372, 380
- Zeldovich, Ya. B., Einasto, J., Shandarin, S., 1982, Nature, 300, 407